Prototype Implementation of an Arduino Mega Based Current Recorder

Waluyo[1†], **Siti Saodah**[2], and **Yogi Wibisono**[1], Non-members

ABSTRACT

Electric current measurements in electric power systems are important aspects that need to be monitored for protection. Therefore, this study designed, implemented, and tested a digital current measuring and recording prototype instrument. The current signals of the loads were sensed by the split-core transformers, which entered the signal conditioning, through the Arduino Mega 2560 microcontroller, and emitted output through a PC monitor, SD card data logger, and LCD. Furthermore, the device was tested with the results compared to the computation and clamp ammeter readings, as the reference values. The testing loads are 1500 W and 500 W for single-phase and per-phase of three-phase systems respectively, due to limitation of the loads. Both single and three-phase systems exhibited an increase and decrease in the absolute and relative deviations, respectively, due to an increase in load.

However, the values in both systems were not the same. For the single-phase, the average absolute and relative deviation slopes were 0.156548 A/kW and −0.0020772 %/kW, respectively. On the other hand, for the three-phase system, they were 0.12372 A/kW and −0.04176 %/kW, respectively. The relative deviations to the computation results were under 6 %, and decreased to 3 %, while the relative deviations to the reference instrument readings were under 3 %, decreased to 1 %, as the load increased. Therefore, the accuracy is within between 1 % and 3 % of that yielded by instruments generally used for measurements.

Keywords: LCD, Measurement, Microcontroller, SD Card, Split-Core

LIST OF SYMBOLS

ADC	Analog-to-digital converter
A_{ref}	The upper limit of voltage that could be read by the microcontroller
CS	Chip select
CT	Current transformer
CT1	First clamp current transformer
CT2	Second clamp current transformer
CT3	Third clamp current transformer
Er01	Single-phase deviation on the reference instrument current readings and the computations
Er02	Single-phase deviation on the average of three-phase LCD current readings and the computations
Er03	Single-phase deviation on the average of three-phase SD card current readings and the computations
Er04	Single-phase deviation on the average of three-phase LCD current readings and the computations
Er05	Single-phase deviation on the average of three-phase SD card current readings and the computations
Er-L1-c	Phase L1 deviations between reference instrument readings and computations
Er-L1-c1	Phase L1 deviations between LCD readings and computations
Er-L1-c2	Phase L1 deviations between SD card readings and computations
Er-L1-r	Phase L1 deviations between LCD readings and reference instrument readings
Er-L1-r1	Phase L1 deviations between SD card readings and reference instrument readings
Er-L2-c	Phase L2 deviations between reference instrument readings and computations
Er-L2-c1	Phase L2 deviations between LCD readings and computations
Er-L2-c2	Phase L2 deviations between SD card readings and computations
Er-L2-r	Phase L2 deviations between LCD readings and reference instrument readings
Er-L2-r1	Phase L2 deviations between SD

Manuscript received on August 25, 2019 ; revised on June 22, 2020 ; accepted on September 24, 2020. This paper was recommended by Associate Editor Nattachote Rugthaicharoencheep.

[1]The authors are with the Department of Electrical Engineering, Institut Teknologi Nasional Bandung, Indonesia.

[2]The author is with the Department of Energy Conversion, Politeknik Negeri Bandung, Indonesia.

[†]Corresponding author: waluyo@itenas.ac.id

Digital Object Identifier 10.37936/ecti-eec.2021191.222588

	card readings and reference instrument readings
Er-L3-c	Phase L3 deviations between reference instrument readings and computations
Er-L3-c1	Phase L3 deviations between LCD readings and computations
Er-L3-c2	Phase L3 deviations between SD card readings and computations
Er-L3-r	Phase L3 deviations between LCD readings and reference instrument readings
Er-L3-r1	Phase L3 deviations between SD card readings and reference instrument readings
GND	Connected to grounding
I2C	Inter IC bus
Iav-c	Average computation
Iav-r	Average reference instrument readings
Iav-LCD	Average LCD readings
Iav-SD	Average SD readings
IDE	Integrated development environment
I_s	Secondary current
I_p	Primary current
I/O	Input-output
LCD	Liquid crystal display
LCD-L1	LCD readings on phase L1
LCD-L2	LCD readings on phase L2
LCD-L3	LCD readings on phase L3
LCD average	Average LCD readings
MISO	Master In Slave Out
MOSI	Master Out Slave In
PC	Personal computer
R_{burden}	Burden resistor
RTC	Real-time clock
SCL/SCK	Serial clock
SD	Secure digital
SDA	Serial data
SD-card L1	SD-card readings on phase L1
SD-card L2	SD-card readings on phase L2
SD-card L3	SD-card readings on phase L3
SD-card average	Average SD-card readings
SPI	Serial Peripheral Interface
USB	Universal serial bus
V_{ref}	Reference voltage
x	Measurement result values
$\hat{x}$	Computation and reference instrument reading values

1. INTRODUCTION

Current measurements are defined as the rate at which electric charges passes through a circuit. It is one of the major contributors in several power applications, such as sensing, controlling, protection, and management system. However, the primary issues associated with it are linearity, accuracy, and flexibility, which is normally measured by using a tank clamp meter method [1]. Electricity is an ubiquitous energy carrier resulting from the existence of charged particles, either statically as an accumulation of charge or dynamically as a current. Therefore, its reliability and security need to be improved. The role of current measurement and its accuracy is extremely important and it must be made safe and affordable [2, 3]. An analog reading type instrument introduces appreciable error, due to the current harmonic distortion on non-linear loads, such as power electronics and switching devices [4, 5]. Active and reactive current components were determined through a microcontroller-based system [6]. The sundry types are used in various applications, such as reactive power controls and distortion compensations [14], power and energy measurements [8–10], electromagnetic interference detection [11], power management [12–14] and photovoltaic maximum power point tracking system [15]. The measuring instruments are occasionally operated with a program, such as C language or Labview [16, 17]. Microcontrollers are primarily used to monitor various parameters, such as voltage, current, frequency, temperature [18], and unbalanced three-phase current [19]. Specifically, Arduino Mega 2560 microcontroller is associated with smart sockets [20], the extraction of venom using electrically simulation method [21], underwater glider applications [22], robotic mapping [23], and bisphenol detection [24].

Based on previous studies, it was necessary to design and implement an alternative current measurement and recording prototype instrument for use with single and three-phase systems. This was tackled and tested by utilizing both the hardware and software ecosystem of Arduino Mega 2560 Rev. 3 microcontroller. Furthermore, measurement of outcomes was displayed in three ways using a personal computer (PC) monitor, a secure digital (SD) card data logger, and a liquid crystal display (LCD). The tests involve comparing and computing the readings on the prototype instrument. The deviations from the reference values were analyzed, based on the loading powers and phase types.

2. DESIGN AND TESTING METHODS

The design of the Arduino Mega 2560 microcontroller is based on the current measurement and recording instrument, which was tested and analyzed prior to being incorporated into our implementation. It is the primary controller which regulates five data processing units, namely three current reading, voltage, and temperature sensors simultaneously. The current reading sensors were mini split-core current transformers, which were used to detect approximately 100 A and the accuracy was $\pm 1\,\%$, according to the datasheet. However, in reality, they are set at a maximum current reading capability of

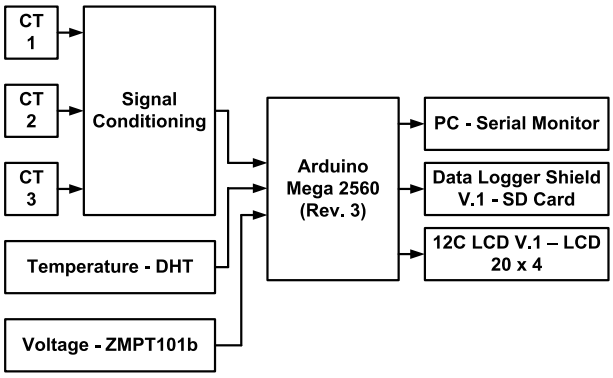

Fig.1: *Measurement and recording instrument diagram.*

20 A, considering the absence of testing load used to measure the high current. However, after processing the data, results were displayed on the LCD screen and recorded in the SD card storage media. The description of the current measurement and recording instrument is indicated by the classification of each part in the block diagram, according to the circuit function, as shown in Fig. 1.

In simple form, Fig. 2 is the flow of data processing units. The first stage is the acquisition of analog data, i.e. the CT capture of line current. This was followed by the analog data conditioning or adjustment. Next, the analog data was converted to digital data. Finally, the data was used to compute absolute and relative deviation analyses.

The current sensors clamped the live conductors, thereby making it unnecessary to disconnect the load wires. The data is either displayed on the LCD screen or PC serial monitor. It is also stored in the SD card. The PC input program in the microcontroller was carried out by the Arduino IDE library software. The uploaded system was used to create a library in order to obtain a flexible instrument, and it can measure both single and three-phase loads.

The power supply board provides an input voltage of 5 V DC. The sensors generated voltages proportional to the measured currents, which were further processed in the signal conditioning circuit to equalize the output voltages with the ADC reading capability limits in the microcontroller. The results from the processed data were displayed on the LCD. The system used the LCD to display the working status of the instrument. The data was also displayed on the PC monitor and stored on the SD card storage medium.

The specification of components dictated the limits and the references in the instrument design. They include Arduino Mega 2560 microcontroller, YHDC SCT-013-000 current sensors, Shield V.1 data logger, I2C V.1 module, 20 × 4 LCD, SD card memory, DHT22 temperature sensor, 12 V/1 A adapter, and 5 main and 3 back-up power supplies.

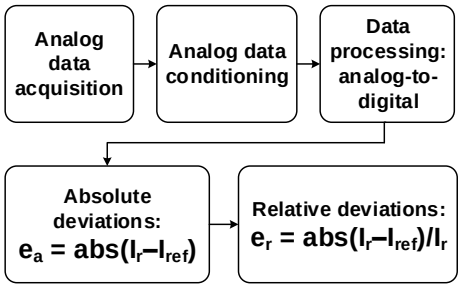

Fig.2: *Data processing.*

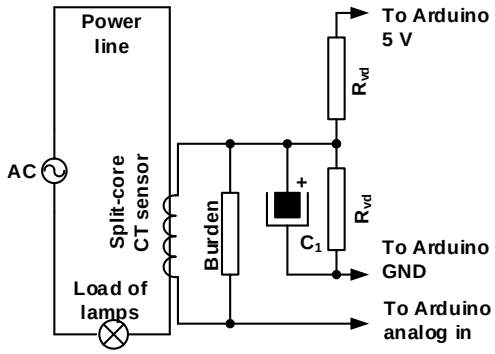

Fig.3: *Signal conditioning circuit.*

The initial step for the prototype design was to create signal conditioning circuits for the supply of current through the sensors. The circuits were intended to transmit negative signals which were converted to positive values by the sensors, and microcontroller, which was only able to read the voltage range of 0–5 volts. Conversely, the AC measurements certainly had negative values during each period. The second step, which is a corrective consideration, involves the testing of sensor readings using the ADC facility on the microcontroller, which is also referred to as the initial calibration stage in the measuring instrument. The final step involves the integration process for data from the five sensors displayed on the LCD and recorded by the logging module.

The signal conditioning circuits served as a regulator of the initial phase because the forms and magnitudes of the sensor output signal were not suitable for the microcontroller ability. They consist of three circuits, which each accommodate one current sensor. The circuit assembly is comprised of a PCB, three female jacks, burden resistors and capacitors, six 360 kΩ resistors, an LED, and a header. The signal conditioning circuit is shown in Fig. 3.

The three circuits were required to determine the burden and the voltage divider resistances. The 2.5 V referred to as the GND reference substitution number was generated by the voltage dividers, in the burden signal conditioning circuit, which serves as the load on the secondary circuit. This voltage generation was

Fig.4: *Current transformers for the prototype instrument.*

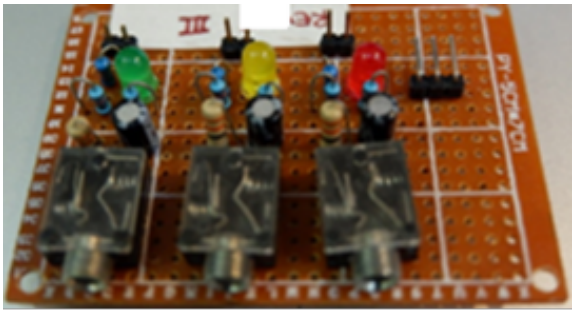

Fig.5: *Assembled signal conditioning circuit.*

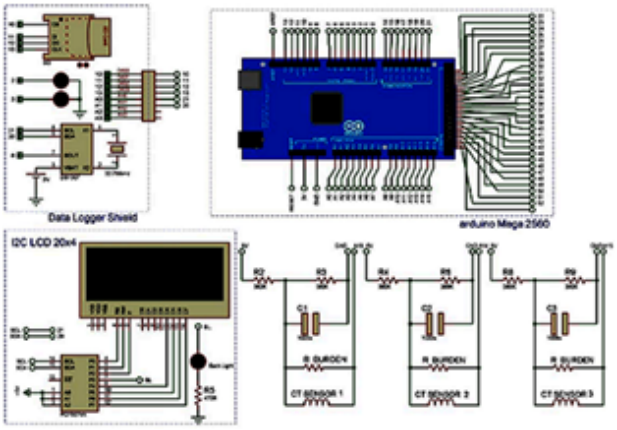

Fig.6: *Hardware integration.*

recently proposed, besides the signal processing in the microcontroller. They were related to the ability of the CT to accept certain impedance limits. The burdens were expressed in impedances. The ratio between secondary (I_s) and primary (I_p) CT currents needs to be calculated before further computations. The primary and secondary currents were 100 A and 50 mA, respectively, and it generated a turn ratio of 2000. The range for the initial sensor reading was from 0 to 100 A, and these values need to be reduced to a range from 0 to 20 A. Therefore, the maximum primary current obtained was 28.284 A. The maximum secondary current was 0.0141 A. Fig. 4 shows the split-core current transformers used for the design measurement instrument.

The signals from the current readings were sine waves, which meant they had positive and negative values alternately. Therefore, the midpoint of sinusoidal voltages needs to be raised in order always to obtain positive values. The midpoints of the current sensor output signals tend to be positive, when raised above zero, namely half of the microcontroller readable voltage limit (V_{ref}) which is 2.5 V. V_{ref} was the new midpoint for the sensor output signals to realize positive values. The voltage limit read by the microcontroller (A_{ref}) was 5 V. The new midpoint of 2.5 V simply implies that the used GND sensor voltage of 0 V was replaced by 2.5 V. Subsequently, the ideal burden resistor of 177 Ω (R_{burden}) was calculated using Ohm's law. Because of its unavailability in the market, a resistor with the nearest value, which is 180 Ω, was selected. A similar reason led to the selection of 20 A. Furthermore, the next phase was the soldering stage, with an R_{vd} of 360 kΩ, which was much higher than the burden resistance, obtained as 2000 ratio. Fig. 5 shows the assembled signal conditioning circuit.

The Arduino Mega 2560 microcontroller was selected since it has a large number of I/O ports. As the name implies, the microcontroller board has an enlarged physical size, and this type is quite popular in the market. It has a Universal Serial Bus (USB) connector, which serves as a data transfer medium as well as the power input and as an external connector that supported the stipulated voltage range, from 6 to 20 V DC. The size of flash memory is 256 kB, making the microcontroller board an option for complex instrumentation projects. Fig. 6 shows the overall schematic hardware integration of the instrument, which consist of the Arduino Mega 2560 microcontroller board, three SCT 013-000 current sensors, I2C module, LCD, and data logger Shield V1.0 module, which is used as the data recorder.

The schematic wiring diagram is simulated by using *Fritzing*. The various components were connected to the microcontroller I/O pins. The list of used pins and connections between them is shown in Table 1. The connections from the microcontroller to the LCD were designed with the I2C module, to protect the pins. In addition, 20 pins were used for SDA (Serial Data) and 21 for SCL (Serial Clock).

The software made it easier to define the library "LiquidCrystal_I2C.h" at the top of the sketch. Furthermore, all functions included in the library, are optimized. Immediately after the program was uploaded, the microcontroller searched for any I2C addresses connected to the board, and this appeared on the monitor.

The LCD required an additional I2C backpack module to protect the I/O pins on the microcontroller. On the contrary, the RTC (Real Time Clock)

Table 1: *Use of Arduino pins.*

Components	Pin description of microcontroller
LCD I2C	Pin GND → Pin GND power supply
	Pin VCC → Pin 5 V power supply
	Pin SDA → Pin D20 Arduino
	Pin SCL → Pin D21 SCL Arduino
Signal conditioning	Pin GND → Pin GND power supply
	Pin VCC → Pin 5 V power supply
	Pin L1 → Pin A13 Arduino
	Pin L2 → Pin A14 Arduino
	Pin L3 → Pin A15 Arduino
Temp. sensor DHT 22	Pin GND → Pin GND Arduino
	Pin VCC → Pin 3.3 V Arduino
	Pin Data → Pin D2 Arduino
Real-time clock	Pin A4 SDA → Pin D20 SDA Arduino
	Pin A5 SCI → Pin D21 SCL Arduino
SD card	Pin D13 SPI Clock → Pin D13 Arduino
	Pin D12 SPI MISO → Pin D12 Arduino
	Pin D11 SPI MOSI → Pin D11 Arduino
	Pin D10 SD Card Chip Select → Pin D10 Arduino
Voltage sensor ZMPT 101B	Pin GND → Pin GND power supply
	Pin VCC → Pin 5 V power supply
	Pin Data → Pin A12 Arduino

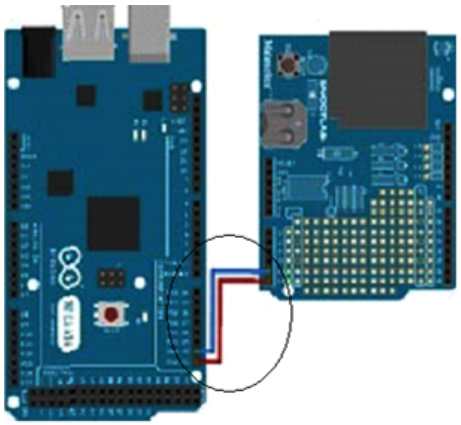

Fig.7: *Pin A4 and A5 in a jumper to pin 20 and 21.*

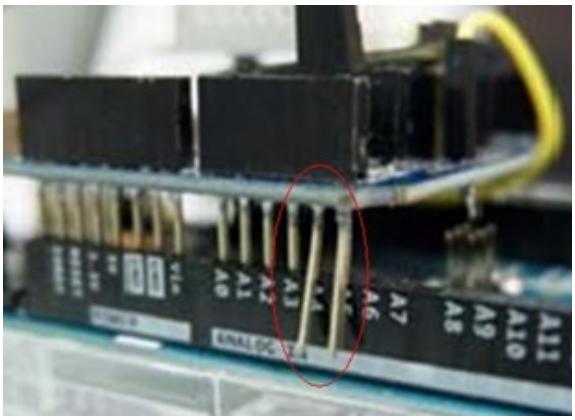

Fig.8: *Pin A4 and A5 modifications on shield module.*

module was embedded in the Logged Shield V1.0 and I2C modules. However, the SDA and SCL pin placements were incompatible with those on the microcontroller.

The SDA and SCL pins were located on A4, and A5 respectively, on the data logging shield module V1.0. Conversely, the SDA and SCL on the microcontroller were located on the pins 20 and 21. However, in order to access the I2C module, the A4 and A5 pins were removed from the microcontroller board. Furthermore, pins A4 and A5 were in a jumper to pins 20 and 21, respectively. Figs. 7 and 8 show the module pins A4 and A5 which were with a jumper to pins 20 and 21.

The RTC was embedded in the data logger shield module of DS1307, in order for the software to be used in the library, and it was accessed using the serial monitor. Accessing the SD card in the V1.0 data logger shield module requires at least 4 pins: #13, #12, #11, and #10 digital pins serving as SPI Clock, SPI MISO, SPI MOSI, and SD card CS respectively. Similarly, in the case of RTC assessment, the used pins in the V1.0 data logger shield module were configured differently, where MOSI, MISO, and SCK pins were placed on digital pins 51, 50, and 13, respectively.

The analog pins 9, 10, and 11 aligned with CT1, CT2, and CT3, respectively in microcontroller were used to access the sensor currents. The CT ratio was divided by the burden resistance, and a calibration value of 11.111 was obtained.

After the design stage, functional and measure-

Fig.9: *LCD test.*

Fig.10: *Microcontroller and signal conditioning output voltages.*

ment tests were carried out to ascertain whether or not the components were operating properly. The measurements were compared based on the computation results and the readings on the reference instrument. Furthermore, the deviations from the reference values need to be considered. The absolute and relative percentage of deviations are computed in Eqs. (1) and (2), respectively [25].

$$e_a = |x - \hat{x}| \tag{1}$$

$$e_r(\%) = \left| \frac{x - \hat{x}}{x} \right| \cdot 100\,\% \tag{2}$$

In this instance, x and $\hat{x}$ denote the measured and reference values respectively.

The three-phase measurements were carried out by connecting five 100 W incandescent lamps in a star-like manner, and the CT was clamped on each phase conductor. The reference instrument was used to measure each current alternately. However, our prototype had three transformers to allow measuring the three-phase currents simultaneously.

3. RESULTS AND DISCUSSION

In the first section, each of the components was tested to ensure, it was functional. Consequently, the LCD testing was carried out by connecting the I2C module to the microcontroller in the subsequent section. However, to ascertain whether the installations were properly connected, the initial designation was marked by the emergence of the LCD light. Further analyses were carried out by ensuring the basic commands on the microcontroller brought up letters or numbers on each column and row, to find out whether the LCD responded. The test output is shown in Fig. 9.

The signal conditioning functional test was used to compare the output voltages as well as to determine

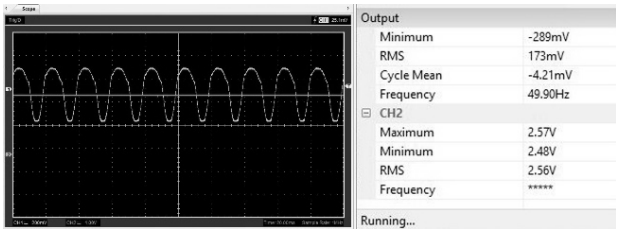

Fig.11: *Signal sample of 400 W load.*

whether the issued signal was safe to be read by the microcontroller. According to Fig. 10, the microcontroller and signal conditioning output DC voltages were functional. The values of the frequency were concealed as a result of the DC voltage signals. The RMS voltages on channels 1 and 2 were 4.77 V and 2.55 V, respectively.

Fig. 11 shows a signal sample of 400 W load. This display revealed mainly the AC voltage and frequency, on channel 1, as 173 mV RMS and 49.9 Hz, respectively. The frequency was invisible in channel 2, while the RMS voltage obtained was 2.56 V.

The signal on the microcontroller was read using a personal computer (PC) oscilloscope because it had an initial value of 0 V, which was raised to a positive value of 2.5 V. It was stated earlier that the microcontroller tends to read-only signal within the range of 0–5 V DC. The testing, which was carried out using the monitor, as a facility of Arduino IDE (Integrated Development Environment) built-in software, functioned to ascertain if the sensors and other components functioned effectively.

These measurements and the recorded data were carried out by monitoring the information on the LCD or the monitor display. A failure in the recording is possible if FAT 32 format was not installed in the SD card or the SD card was unplugged.

In carrying out current reading and recording tests, the yielded data was compared to the readings on the reference instrument. In this prototype, the resistive loads consisted of 15 incandescent lamps, each with 100 W. In the three-phase testing, the load on each phase used approximately one to five lamps. In contrast, the single-phase testing used approximately one to fifteen incandescent lamps. Fig. 12 shows the single-phase current measurement and its recording, using our instrument prototype. In this testing, the three split-core CTs were jointly installed on the live wire.

Fig. 13 shows the line graphs of testing results on the reference instrument, as well as our prototype's readings, and their comparisons. The graph shows that both the computed and measured values of the single-phase load did not form tangential curves to the end. The computed currents had higher values than the readings on the reference instrument. This was likely caused by the fact that the specified data

Fig.12: *Single-phase current measurement and recording.*

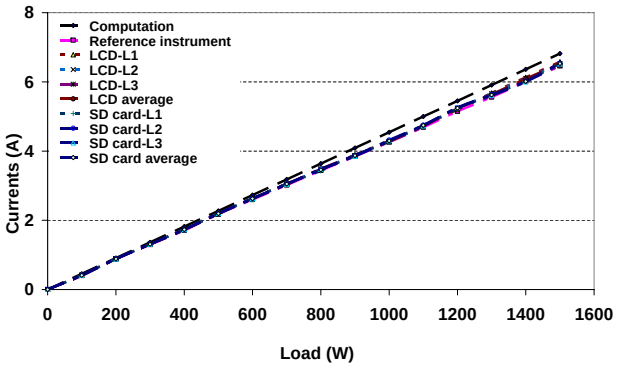

Fig.13: *Comparison of single-phase computations and measurements.*

from the phase-to-neutral voltages and the active unity power factor were ideal. Conversely, the data from the measuring instrument was based on the flow of current at that time, and it was strongly influenced by the voltage, load resistance, real power factor, and temperature. The computation, reference instrument, LCD-L1, LCD-L2, LCD-L3, LCD average, SD card-L1, SD card-L2, SD card-L3, and SD card average notations represent the values of current based on the computations, readings from the reference instrument, LCD and SD-card readings on L1, L2, L3 phases and their respective averages. This shows that an increase in the load lead to a slight increase in deviation. However, this condition is normal.

Fig. 14(a) shows the deviation line graphs for the single-phase measurements. The first line on the graph (Er01) was the deviation between the current readings on the reference instrument and the computation results. This shows that the line graph was the highest among the remaining ones. The second line on the graph (Er02) was the deviation

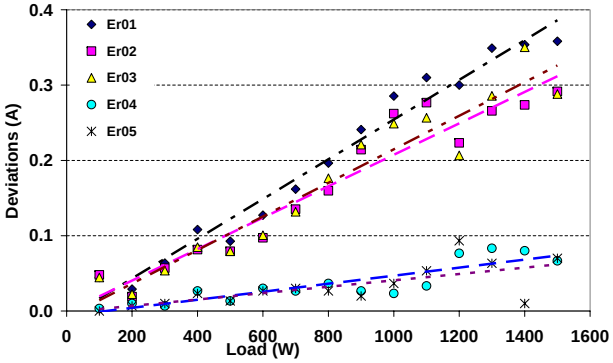

(a) Absolute deviations

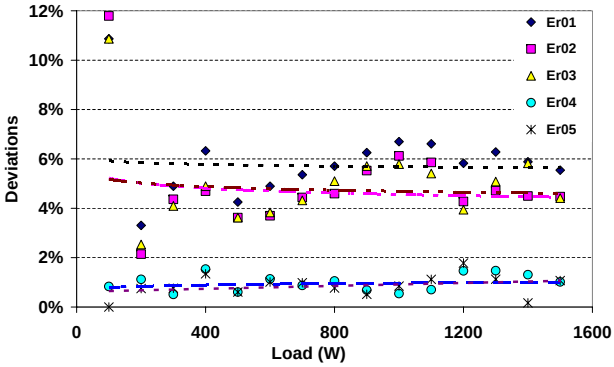

(b) Relative deviations

Fig.14: *Deviations of single-phase measurements.*

between the average LCD current readings on three phases and the computed results, and this occupied the third-highest line graph. The third line on the graph (Er03) was the deviation between the average SD-card current readings from the three phases, and the yielded computed results. The fourth line on the graph (Er04) was the deviation between the average current on the three phases and the readings on the reference instrument, and this occupied the fourth-highest line graph. The fifth line on the graph (Er05) was the deviation between the average SD-card current on the three phases and the readings from the reference instrument, and it occupied the fifth, and final line graph. The Er01, Er03, and Er02 lines on the graph have a considerably high slope, while the remaining two had significantly lower slopes. Therefore, the absolute deviations of measurements tend to rise as the load increases. However, the deviations were extremely low on the actual currents.

Fig. 14(b) shows the percentage graph of deviations on the single-phase measurements. The slopes of Er01, Er02, and Er03 decreased gently, while the remaining graphs were constant. Therefore, it is clear that there was a slight decrease in the percentages of deviations as the load increased.

Table 2 shows a list of the average slopes from the Er01, Er02, Er03, Er04, and Er05 lines on

Table 2: *Average deviation slopes of single-phase.*

No.	Absolute deviation slopes (A/kW)	Relative deviation slopes (%/kW)
Er01	0.26373	−0.001885
Er02	0.20873	−0.008706
Er03	0.22278	−0.004853
Er04	0.04512	0.002091
Er05	0.04238	0.002967
Average	0.156548	−0.0020772

Fig.15: *Three-phase current measurements.*

the graph, in the absolute (A/kW) and the relative deviations (%/kW). The average absolute deviations for Er01, Er02, and Er03 are 0.26373, 0.20873, and 0.22278 A/kW, respectively, and they were considered to be significant. This simply means that they tend to rise whenever there was an increase in the currents and load. Nevertheless, the average relative deviation for the slopes were −0.001885, −0.008706, and −0.004853 %/kW, respectively. It shows that the average relative deviation tends to reduce slightly as the load and currents increased.

Furthermore, the average absolute deviation for the slopes of Er04 and Er05 were 0.04511 and 0.04238 A/kW, respectively, and they were considered to be fairly low. It means that they increased slightly when there as an increase in current and load. Subsequently, the average relative deviations for Er04 and Er05 are 0.00209 and 0.002967 %/kW, respectively. In addition, both slopes had low values because the increments of deviations were extremely low.

Fig. 15 shows the three-phase current measurement and recording process using our instrument prototype. The clamp CTs were simultaneously installed in each phase.

Fig. 16 is a sample of the three-phase current measurements. The time, temperature, three-phase currents, and voltage were properly recorded.

In the three-phase measurements, a maximum of five incandescent lamps in each phase was connected in a star-like (wye) manner. The CT was attached to

19:06:18	26.0 C	2.34 A	2.16 A	2.22 A	215.3 V
19:06:19	26.0 C	2.34 A	2.17 A	2.23 A	215.3 V
19:06:20	26.0 C	2.33 A	2.18 A	2.21 A	215.3 V
19:06:20	26.0 C	2.31 A	2.18 A	2.23 A	215.3 V
19:06:21	26.0 C	2.31 A	2.18 A	2.23 A	215.3 V
19:06:22	26.0 C	2.33 A	2.16 A	2.22 A	215.3 V
19:06:23	26.0 C	2.33 A	2.18 A	2.20 A	215.3 V
19:06:24	26.0 C	2.34 A	2.17 A	2.21 A	215.3 V
19:06:25	26.0 C	2.31 A	2.17 A	2.23 A	215.3 V
19:06:25	26.0 C	2.33 A	2.16 A	2.23 A	215.3 V
19:06:26	26.1 C	2.34 A	2.16 A	2.22 A	215.3 V
19:06:27	26.1 C	2.33 A	2.18 A	2.20 A	215.3 V
19:06:28	26.1 C	2.31 A	2.17 A	2.23 A	215.3 V
19:06:28	26.1 C	2.31 A	2.16 A	2.23 A	215.3 V
19:06:29	26.1 C	2.34 A	2.17 A	2.20 A	215.3 V
19:06:30	26.1 C	2.31 A	2.18 A	2.22 A	215.3 V
19:06:31	26.1 C	2.32 A	2.18 A	2.23 A	215.3 V

Fig.16: *Sample of the three-phase current recording.*

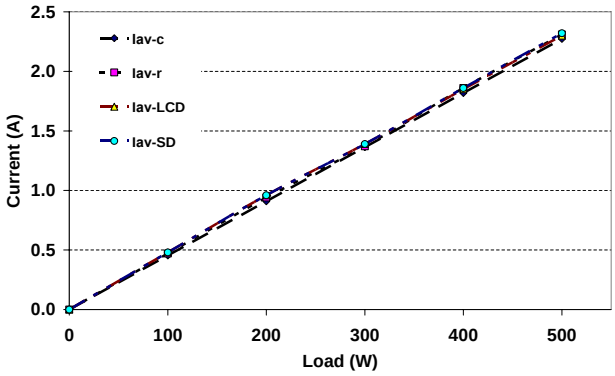

Fig.17: *Average three-phase current computation and measurement results.*

every conductor that led to the load. The reference instrument was used to measure each conductor alternatively. Our instrument prototype, three CTs were used to measure the currents generated by the incandescent lamps simultaneously.

Fig. 17 shows the average results from the three-phase testing as well as the comparison of current readings obtained from the reference instrument and our prototype. Iav-c, Iav-r, Iav-LCD, and Iac-SD represented the average computation, reference instrument, LCD, and SD card readings, respectively.

Fig. 18(a) shows the absolute deviations of the phase-L1 computation and measurement results. Er-L1-c, Er-L1-c1, Er-L1-c2, Er-L1-r, and Er-L1-r1 represented the absolute deviations between the reference instrument readings and the computations, the LCD readings and computations, the SD card readings and the computations, the LCD readings and the reference instrument readings, and the SD card readings and the reference instrument readings, respectively. Generally, the Er-L1-c and Er-L1-c2 had significant rising slopes. Conversely, the rest had slightly reduced slopes. Furthermore, the Er-L1-c2 slope had the highest average deviation of 0.0384 A among the rest graphs. While, the

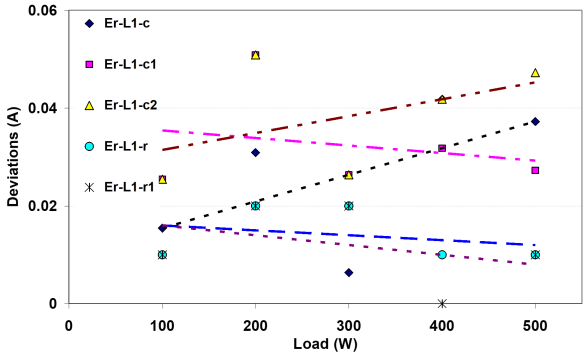

(a) Absolute deviations

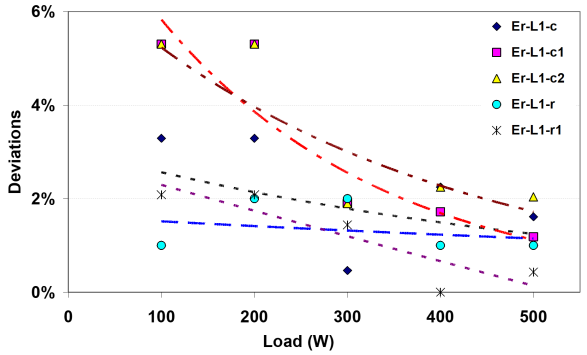

(b) Relative deviations

Fig.18: *Deviations of phase-L1 current measurements.*

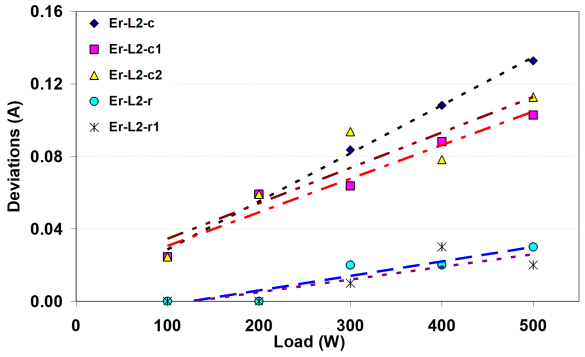

(a) Absolute deviations

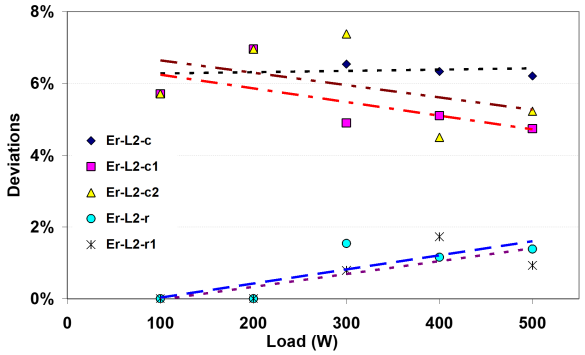

(b) Relative deviations

Fig.19: *Deviations of phase-L2 current measurements.*

Er-L1-c, Er-L1-c1, Er-L1-r, and Er-L1-r1 had the average deviations of 0.02636 A, 0.0324 A, 0.0140A, and 0.0120 A, respectively.

Fig. 18(b) shows the graphs of relative deviations for phase-L1 current measurements. All these graphs tend to reduce as the load increases. Furthermore, the average slopes were all different from each other.

Fig. 19(a) shows the absolute deviations of phase-L2 current measurements. The notations are similar to Fig. 18(a), except for phase-L2. Generally, the deviations rose as the load increased, with different slope levels. The first, third, and second graphs are significant, while the fourth and fifth graphs had slight slope levels.

Furthermore, Fig. 19(b) shows the relative deviations of phase-L2 current measurements. Generally, there were slight increases and reductions in the slopes. There was a considerable decrease in the first, second, and third curves and a slight increase in the fourth and fifth curves.

Fig. 20(a) shows the absolute deviations of phase-L3 graph. There were considerable increases in the slopes of the first, second, third, and fourth curves. Conversely, there was a slight decrease in the slope level of the fourth curve.

Fig. 20(b) shows the relative deviations of phase-L3 current measurements. Generally, there were decreases in deviations as the load increased.

Table 3: *Three-phase deviation slopes.*

Deviations	Absolute deviation slope (A/kW)			Relative deviation slope (%/kW)		
	L1	L2	L3	L1	L2	L3
Er-c	0.0545	0.2655	0.0736	−0.0439	0.0036	−0.0187
Er-c1	−0.0155	0.1855	0.0555	−0.1182	−0.0380	−0.0702
Er-c2	0.0345	0.1955	0.1055	−0.0959	−0.0344	−0.0742
Er-r	−0.0100	0.0800	−0.0200	−0.0100	0.0392	−0.0520
Er-r1	−0.0200	0.0700	0.0300	−0.0539	0.0358	−0.0569

Table 3 summarises the absolute and relative three-phase deviations slopes. The absolute deviations possess significant positive values. In contrast, the relative deviation slopes were dominated by slightly negative values.

The absolute deviations of the average three-phase current measurements increase with an increase in the load. Certain differences were detected in the slopes. Based on Fig. 21, the third graph, which shows the deviation between the SD card current readings and its computation, had a significant slope value. The others were quite similar, and this phenomenon is shown in Fig. 21(a).

Fig. 21(b) shows the relative deviations of the

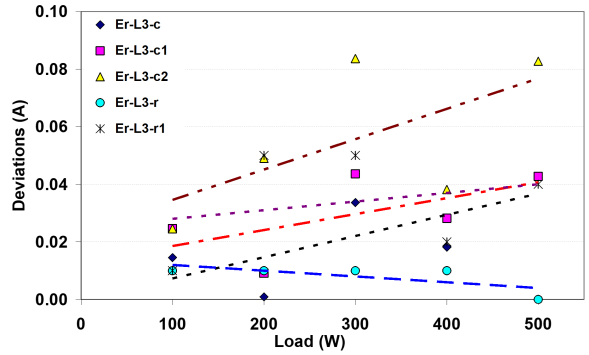

(a) Absolute deviations

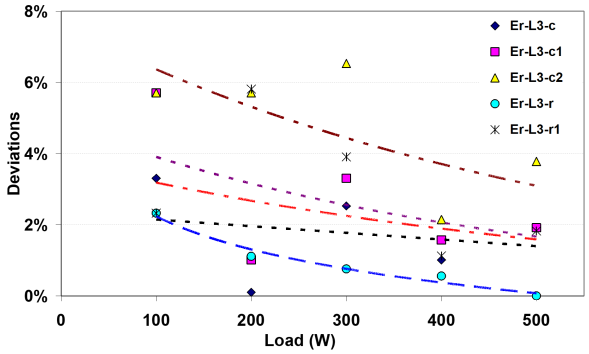

(b) Relative deviations

Fig.20: *Deviations of phase-L3 current measurements.*

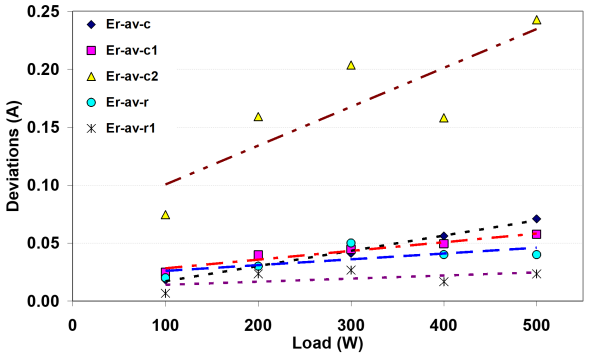

(a) Absolute deviations

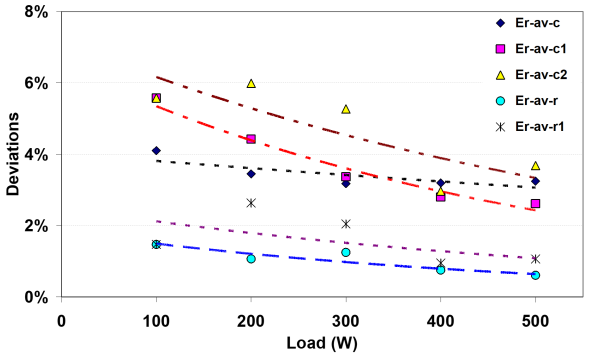

(b) Relative deviations

Fig.21: *Deviations of average three-phase current measurements.*

average three-phase current measurements. It clearly shows that there was a slight reduction in all of them as the load increased.

Table 4 summarises the average absolute and relative three-phase deviation slopes. The average absolute deviation had positive values, which implies that an increase in measurements also led to an increase in the load. The average relative deviation had negative values, which shows that it reduces as the load increases. Generally, the average relative deviation slopes for the remaining quantities and the reference instrument readings were extremely low. This shows that the readings from our prototype were similar to the results from the actual measurement.

In the tests, there were differences between the results from the computation, the readings obtained from the reference instrument, and our prototype. This was because the ideal computation data based on the resistive load from the incandescent lamps was used. Another perfect condition was the 220 V phase-to-neutral constant voltage source. However, the actual voltages obtained during the measurements always varied slightly. Besides that, the different brands and types of incandescent lamps used led to the existence of dissimilarities between the computations and direct measurements using the reference instrument. In addition, they were probably

Table 4: *Average three-phase deviation slopes.*

Deviations	Average absolute deviation slope (A/kW)	Average relative deviation slopes (%/kW)
Er-av-c	0.1312	−0.0197
Er-av-c1	0.0752	−0.0755
Er-av-c2	0.3355	−0.0682
Er-av-r	0.0500	−0.0204
Er-av-r1	0.0267	−0.0250
Average	0.12372	−0.04176

caused by only one CT, while three of them are required. Consequently, during measurements, the reference instrument needs to measure each phase conductor with respect to time. Our prototype already had three CTs, which made it possible for them to measure the currents on the three-phase conductors simultaneously.

Based on the current readings from the reference instrument, the LCD, and our prototype, on the single-phase L1, L2, or L3, the deviations were discovered to be much smaller than the result from previous calculation. This was probably caused by using the same measurement methods for obtaining current readings, such as CTs, as the linkage between magnetic induction and closed electrical

circuits, as well as converting the outcome to a lower value. The electric currents were converted to the voltages, corresponding to the limits of the microcontroller, which was further used to process the data to be displayed on the LCD for each measuring instrument. This behavior was similar to that of the three-phase measurements, and the difference was that the reference instrument measured the currents alternately.

The errors in our prototype were possibly reduced by using a more precise voltage divider resistor when designing the signal conditioning and the use of an effective voltage regulator. The output voltage of the microcontroller was precisely at 5 V DC.

4. CONCLUSION

Based on our instrument prototype design and testing carried out by utilizing Arduino Mega 2560 microcontroller, we conclude that the analog data originating from CTs was successfully converted to digital and displayed on the 20×4 LCD screen. In addition, the measurement results were recorded on the SD card medium.

Generally, in both the single and three-phase systems, whenever there was an increase in the absolute deviations, a slight decrease is recorded in the relative ones as the load increases. However, the values in both systems are dissimilar. Subsequently, the average absolute and relative deviation slopes were 0.156548 A/kW and −0.0020772 %/kW, respectively, for the single phase. In contrast, 0.12372 A/kW and −0.04176 %/kW were obtained, respectively, for the three-phase system. The relative deviations from the computation results were below 6 %, at approximately 3 %, while the readings from the reference instrument were below 3 %, relatively 1 %, as the load increased to 500 W per phase. Thus, the prototype is viable for practical measurements.

References

[1] A. M. Patel, "Current Measurement in Power Electronics and Motor Drive Applications – A Comprehensive Study," M.S. thesis, University of Missouri-Rolla, Rolla, MO, USA, 2007.

[2] O. Krejcar and R. Frischer, "Real-Time Voltage and Current Phase Shift Analyzer for Power Saving Applications," *Sensors*, vol. 12, no. 8, pp. 11391–11405, 2012.

[3] M. J. Mnati, R. F. Chisab, and A. Van den Bossche, "A Smart Distance Power Electronics Measurement Using Smartphone Applications," in *2017 19th European Conference on Power Electronics and Applications (EPE'17 ECCE Europe)*, 2017, pp. P.1–P.11.

[4] U. B. Mujumdar and J. S. Joshi, "Microcontroller based true RMS current measurement under harmonic conditions," in *2010 IEEE International Conference on Sustainable Energy Technologies (ICSET)*, Kandy, Sri Lanka, 2010.

[5] S. Rustemli and M. Ates, "Measurement and Simulation of Power Factor using PIC16F877," *Przegląd Elektrotechniczny (Electrical Review)*, vol. 88, no. 6, pp. 290–294, 2012.

[6] M. A. Anadol, M. Aydin, and T. Yalçinöz, "A real-time extraction of active and reactive current using microcontrollers for a multi-pulse STATCOM," *Turkish Journal of Electrical Engineering and Computer Science*, vol. 21, no. 4, pp. 1044–1060, 2013.

[7] P. Doulai and G. Ledwich, "Microcontroller-based Strategy for Reactive Power Control and Distortion Compensation," *IEE Proceedings B (Electric Power Applications)*, vol. 137, no. 6, pp. 364–372, Nov. 1990.

[8] B. Belvedere, M. Bianchi, A. Borghetti, C. A. Nucci, M. Paolone, and A. Peretto, "A Microcontroller-Based Power Management System for Standalone Microgrids With Hybrid Power Supply," *IEEE Transactions on Sustainable Energy*, vol. 3, no. 3, pp. 422–431, July 2012.

[9] P. Srividyadevi, D. V. Pusphalatha, and P. M. Sharma, "Measurement of Power and Energy Using Arduino," *Research Journal of Engineering Sciences*, vol. 2, no. 10, pp. 10–15, Oct. 2013.

[10] A. Ozdemir and A. Ferikoglu, "Low cost mixed-signal microcontroller based power measurement technique," *IEE Proceedings - Science, Measurement and Technology*, vol. 151, no. 4, pp. 253–258, July 2004.

[11] F. Wan, F. Duval, X. Savatier, A. Louis, and B. Mazari, "Electromagnetic interference detection method to increase the immunity of a microcontroller-based system in a complex electromagnetic environment," *IET Science, Measurement & Technology*, vol. 6, no. 4, pp. 254–260, July 2012.

[12] J. W. Andrew, B. Narayanan, and P. B. Murugan, "An Intelligent Uninterrupted Isolated Power Management System Based on ARM Microcontroller," in *Third International on Sustainable Energy and Intelligent Systems (SEISCON 2012)*, Tiruchengode, India, 2012.

[13] Q. I. Ali, "Event-driven duty cycling: an efficient power management scheme for a solar-energy harvested roadside unit," *IET Electrical Systems in Transportation*, vol. 6, no. 3, pp. 222–235, Sep. 2016.

[14] R. Subha and S. Himavathi, "Active power control of a photovoltaic system without energy storage using neural network-based estimator and modified P&O algorithm," *IET Generation, Transmission & Distribution*, vol. 12, no. 4, pp. 927–934, Feb. 2018.

[15] A. A. Elbaset, H. Ali, M. A. Sattar, and M. Khaled, "Implementation of a Modified Perturb

and Observe Maximum Power Point Tracking Algorithm for Photovoltaic System using an Embedded Microcontroller," *IET Renewable Power Generation*, vol. 10, no. 4, pp. 551–560, Apr. 2016.

[16] R. W. Fransiska, E. M. P. Septia, W. K. Vessabhu, W. Frans, W. Abednego and Hendro, "Electrical Power Measurement using Arduino Uno Microcontroller and LabVIEW," in *2013 3rd International Conference on Instrumentation, Communications, Information Technology and Biomedical Engineering (ICICI-BME)*, Bandung, Indonesia, 2013, pp. 226–229.

[17] T. Ahamed and A. Sreedevi, "Design and Development of PIC Microcontroller Based 3 Phase Energy Meter," *International Journal of Innovative Research in Science, Engineering and Technology*, vol. 3, special issue 1, pp. 1370–1379, Feb. 2014.

[18] M. Anand, R. Sumi, G. Nithya, and B. Mahalakshmi, "Microcontroller Based Transformer Monitoring and Controlling System Using Zigbee," *International Journal of Advanced Research in Electronics and Communication Engineering (IJARECE)*, vol. 3, no. 12, pp. 1876–1884, Dec. 2014.

[19] B. Suprianto and L. A. Subagyo, "Control System Of Current Flow 3-Phase Unbalanced Based On Arduino Uno," *International Journal of Engineering and Applied Sciences (IJEAS)*, vol. 4, no. 9, pp. 35–40, Sep. 2017.

[20] A. N. Santos, M. A. A. Macabuhay, and J. N. De Leon, "Smart Household Socket with Power Monitoring & Control using Android Application," in *2017 9th IEEE-GCC Conference and Exhibition (GCCCE)*, Manama, Bahrain, 2017.

[21] T. Besson, D. Debayle, S. Diochot, M. Salinas, and E. Lingueglia, "Low cost venom extractor based on Arduino® board for electrical venom extraction from arthropods and other small animals," *Toxicon*, vol. 118, pp. 156–161, Aug. 2016..

[22] J. Busquets-Mataix, J. V. Busquets-Mataix, and D. Busquets-Mataix, "Combined Gas-Fluid Buoyancy System for Improved Attitude and Maneuverability Control for Application in Underwater Gliders," *IFAC-PapersOnLine*, vol. 48, no. 2, pp. 281–287, 2015.

[23] A. H. Zakaria, Y. M. Mustafah, J. Abdullah, N. Khair, and T. Abdullah, "Development of Autonomous Radiation Mapping Robot," *Procedia Computer Science*, vol. 105, pp. 81–86, 2017.

[24] H. J. Lim, B. Chua, and A. Son, "Detection of bisphenol A using palm-size NanoAptamer analyzer," *Biosensors and Bioelectronics*, vol. 94, pp. 10–18, Aug. 2017.

[25] J. H. Mathews and K.D. Fink, *Numerical Methods using Matlab*, 3rd ed., Prentice-Hall, 1999, pp. 26–26.

Waluyo received his Bachelor of Engineering degree in Power Electrical Engineering from Institut Teknologi Bandung (ITB), Department of Electrical Engineering in Bandung, Indonesia, in 1994. He received his Master and Doctoral degrees in electrical engineering from the same university, in 2002 and 2010 respectively. He now works as an academic staff (lecturer) at the Department of Electrical Engineering, Institut Teknologi Nasional Bandung. His research interests concern: high voltage engineering, transformers, and power system transmission.

Siti Saodah received her Bachelor of Engineering degree in Power Electrical Engineering from Institut Teknologi Nasional Bandung, Department of Electrical Engineering in Bandung (Indonesia), in 2001. She received her Master's degree in electrical engineering from Institut Teknologi Bandung (ITB), in 2006. She now works as a member of the academic staff (lecturer) at the Department of Energy Conversion, Politeknik Negeri Bandung. Her research interests concern: high voltage engineering, transformer, and electric machines.

Yogi Wibisono is an alumnus from the Department of Electrical Engineering, Institut Teknologi Nasional Bandung, in Bandung, Indonesia. He now works as a member of the engineering staff at a private company. His areas of interest include: electrical engineering, electronics, and measurements.